

EXPERIMENTAL CONSTRAINTS ON THE WETTING OF CHROMITE BY SULFIDE LIQUID

JAMES M. BRENNAN[§] AND LESLEY A. ROSE

Department of Geology, University of Toronto, Toronto, Ontario M5S 3B1, Canada

ABSTRACT

We have determined the wetting properties of Fe-(±Ni,Cu,Co)-S-O melts against chromite in experiments performed at 1300°C using C-O-S gas mixtures to control oxygen and sulfur fugacities [$f(\text{O}_2)$ and $f(\text{S}_2)$, respectively]. Products of experiments at $f(\text{O}_2) = 10^{-8.1}$ and $10^{-8.8}$ produced “wetting” textures, as all dihedral angles between chromite and sulfide melt fall near or below the critical value of 60°, regardless of the identity or quantity of non-ferrous metal within the sulfide melt. Experiments performed at a $f(\text{O}_2)$ of $10^{-9.5}$ yielded uniformly higher dihedral angles compared with experiments performed at higher $f(\text{O}_2)$ with comparable metal contents. Dihedral angles between chromite and sulfide melt increase with increasing non-ferrous metal content, and decrease with the mole fraction of iron and oxygen in the sulfide melt. In this context, we interpret the variation in dihedral angles with melt composition as a consequence of the availability of surface-active iron oxide species. Comparison of previously determined dihedral angles between olivine and sulfide melt with values for chromite reported in this study reveals uniformly lower values of θ for chromite at similar $f(\text{O}_2)$, $f(\text{S}_2)$ and melt composition. In some experiments, we have also observed macroscopically “dry” olivine–chromite triple junctions, suggesting that the olivine–chromite interface can represent a lower-energy configuration compared to olivine or chromite in contact with sulfide melt. Such results suggest that chromite-rich rocks may be highly permeable in the presence of sulfide liquid at the $f(\text{O}_2)$ – $f(\text{S}_2)$ conditions relevant to terrestrial mafic magmas, although interstitial silicates may serve to reduce melt connectivity. Given the overall wettability of chromite by molten sulfide, chromitites in stratiform intrusions or ophiolites will be susceptible to infiltration metasomatism by sulfide liquid, thus serving to enhance their tenor. Infiltration of late-stage, PGE-undersaturated sulfide liquid could also explain the absence of interstitial Ru–Os–Ir-bearing platinum-group minerals in chromitites that contain them as intracrystalline inclusions.

Keywords: chromite, sulfide melt, wetting properties, platinum-group minerals.

SOMMAIRE

Nous avons déterminé l’abilité que possède un bain fondu sulfuré Fe-(±Ni,Cu,Co)-S-O de mouiller la chromite dans des expériences à 1300°C utilisant un mélange de gaz C-O-S afin de fixer les fugacités d’oxygène et de soufre, [$f(\text{O}_2)$ et $f(\text{S}_2)$, respectivement]. Les produits de ces expériences à $f(\text{O}_2) = 10^{-8.1}$ et $10^{-8.8}$ montrent des textures de “mouillage”, c’est-à-dire que les angles diédriques entre la chromite et le liquide sulfuré se rapprochent (ou sont inférieurs à) la valeur critique de 60°, quelle que soit l’identité ou la quantité de métal non-ferreux dans le liquide sulfuré. Des expériences à une $f(\text{O}_2)$ de $10^{-9.5}$ ont produit des angles diédriques plus élevés par rapport aux expériences à plus fortes valeurs de $f(\text{O}_2)$ pour des teneurs comparables en métaux. Les angles diédriques entre chromite et liquide sulfuré augmentent avec une augmentation en teneur en métal autre que le fer, et diminuent avec la proportion de fer et d’oxygène dans le liquide sulfuré. Nous voyons la variation dans les angles diédriques avec la composition du liquide comme conséquence de la disponibilité d’une espèce dissoute contenant fer et oxygène et affectant les propriétés de la surface. Une comparaison des résultats obtenus sur les angles diédriques entre olivine et bain fondu sulfuré avec les valeurs sur la chromite révèle des valeurs uniformément plus faibles de θ pour la chromite à des valeurs semblables de $f(\text{O}_2)$, $f(\text{S}_2)$ et composition du liquide. Dans certaines expériences, nous avons aussi observé des points triples olivine–chromite macroscopiquement “secs”, ce qui laisse supposer que l’interface olivine–chromite peut représenter un agencement à faible énergie de surface comparé à la situation avec l’olivine ou la chromite en contact avec le liquide sulfuré. De tels résultats montrent que les roches riches en chromite pourraient s’avérer très perméables en présence d’un liquide sulfuré aux conditions $f(\text{O}_2)$ – $f(\text{S}_2)$ appropriées pour les magmas mafiques terrestres, quoique les silicates interstitiels pourraient réduire la continuité des domaines de liquide. Compte tenu de l’abilité que possède un liquide sulfuré de mouiller la chromite, les chromitites des massifs stratiformes ou des ophiolites seraient susceptibles d’une métasomatose par infiltration d’un liquide sulfuré, augmentant ainsi leur intérêt économique. L’infiltration tardive d’un liquide sulfuré sous-saturé en éléments du groupe du platine pourrait expliquer l’absence de minéraux interstitiels contenant Ru, Os et Ir dans les chromitites qui les contiennent en inclusions intracrystallines.

(Traduit par la Rédaction)

Mots-clés: chromite, liquide sulfuré, propriétés de mouillage, minéraux du groupe du platine.

[§] E-mail address: brenan@geology.utoronto.ca

INTRODUCTION

Immiscible sulfide liquids play an important role in controlling the dispersal of transition metals and platinum-group elements in the crust and upper mantle. Knowledge of the wetting properties of such melts allows accurate prediction of their topology on the grain-scale, which in turn provides insight into the mechanisms for migration of the sulfide liquid, and whether the final distribution of sulfide is likely to be disseminated or whether the sulfide is massive. In the ideal case, the so-called wetting angle (θ) is a measure of the extent to which a small fraction of melt forms a continuous network of grain-edge tubules, thus allowing for melt flow and separation (Watson & Brenan 1987). Melts are interconnected at all fractions for $\theta < 60^\circ$ (see below). Past work has focused on documenting values of θ for molten sulfide against silicate minerals like the Mg_2SiO_4 polymorphs (olivine, wadsleyite and γ -phase) and MgSiO_3 in the perovskite structure-type (e.g., Ballhaus & Ellis 1996, Minarik *et al.* 1996, Shannon & Agee 1996, 1998, Gaetani & Grove 1999, Rose & Brenan 2001), but there are currently no data available for other minerals that crystallize from mafic magmas. This lack limits our understanding of sulfide distribution in olivine-poor rocks. In this communication, we present the results of experiments designed to document the wetting behavior of Fe ($\pm\text{Ni,Cu,Co}$)-S-O melt against chromite at a high temperature and controlled oxygen and sulfur fugacity [$f(\text{O}_2)$ and $f(\text{S}_2)$, respectively]. Our main interest in the wetting properties of chromite derives from the observation that this phase may precipitate in quantity from mafic magmas as a consequence of magma mixing (e.g., Irvine 1977, Irvine *et al.* 1983) or wall-rock interaction (e.g., Zhou *et al.* 1996, Zhou & Robinson 1997). Chromitites thus formed occur as discontinuous layers or lenses, which may serve as sites of melt collection or dispersion, thereby achieving local importance in affecting the mobility and distribution of sulfide melt in mafic and ultramafic bodies. Moreover, the extent to which chromite is wetted by sulfide melt can also be used to predict whether the interstitial base-metal sulfide present in some chromitites represents sulfide liquid trapped at the time of chromite crystallization, or whether such melt could have infiltrated subsequent to chromite formation. This information bears on the development of models for the platinum-group-element (PGE) mineralization that characterizes some chromitites, particularly with respect to the timing of precipitation of included platinum-group minerals (PGM; Merkle 1992, Brenan & Andrews 2001).

BACKGROUND INFORMATION

The local distribution of a melt phase within a coexisting solid matrix is controlled by the relative energies of the solid-melt and solid-solid interfaces. Subject to

the conditions of both mechanical and chemical equilibrium, and assuming that the surface energy of the mineral grains that comprise the solid matrix is isotropic, the three-dimensional topology of the melt can be predicted with knowledge of the cross-sectional geometry of the solid-melt junction (see Watson & Brenan 1987). The dihedral angle (θ) is defined as the angle formed by two intersecting walls of a melt-filled pore at a junction with two solid grains (Fig. 1). The magnitude of θ is determined by the amount of solid-melt contact required to minimize the total surface-energy of the system, and is expressed by the relation:

$$\theta = 2 \arcsin (\gamma_{\text{SS}} / 2 \gamma_{\text{SM}}) \quad (1)$$

where γ_{SS} and γ_{SM} are the solid-solid and solid-melt surface energies, respectively.

Where $\theta < 60^\circ$, the melt is considered to be "wetting" and if $\theta > 0^\circ$, the melt occupies prismatic grain-edge channels, thus producing an interconnected melt phase in three dimensions, even at low melt-fractions (i.e., $\ll 1$ vol.%; von Bargen & Waff 1986). As the dihedral angle decreases, the grain-edge prisms flatten, reducing the amount of grain-grain contact, and where $\theta = 0^\circ$, the melt covers the grain faces, forming a continuous film. Values of $\theta < 60^\circ$ also indicate that the presence of a small amount of grain-edge melt represents a reduction in surface energy relative to the melt-free case, thus providing the thermodynamic driving force for surface-tension-driven infiltration (Watson 1982, Jurewicz & Watson 1984), a process that results in melt permeation of dry rock in the absence of pre-existing porosity, or pressure gradients. Where $\theta > 60^\circ$, the melt is considered "non-wetting" and grain edges become dry as a result of the liquid phase "beading-up" at grain-edge intersections. For $\theta > 60^\circ$, melt connectivity is achieved only above a finite fraction (i.e., 2 vol.% for $\theta = 65^\circ$; von Bargen & Waff 1986), and spontaneous infiltration of melt does not occur.

EXPERIMENTAL AND ANALYTICAL METHODS

Values of θ were measured in experiments that employed compositions of sulfide melt chosen to reflect the variation seen in natural sulfide globules from volcanic rocks, which offer the best-preserved samples of immiscible sulfide liquids (see the summary in Rose & Brenan 2001). As such, we used an Fe-S base composition, to which varying levels of Ni, Cu and Co were added, to assess their effects on chromite wetting. Oxygen and sulfur fugacities imposed on experiments are consistent with values recorded in natural basalts (e.g., Wallace & Carmichael 1992), thus allowing direct application of our results to a model of the solidification of mafic magmas.

Experiments were conducted in a modified 1-atm vertical tube furnace using mixtures of CO, CO₂, and SO₂ gases to control the fugacities of oxygen and sulfur.

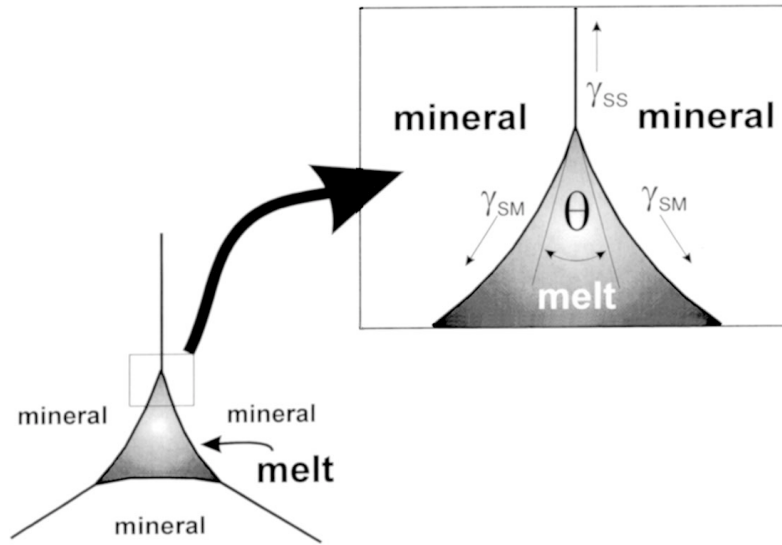


FIG. 1. Schematic illustration of the geometric relations between interfaces exposed in a cross-section through a melt-filled pore (modified after Watson *et al.* 1990). The angle between the mineral–mineral (SS) and mineral–melt (SM) interfaces (θ) is dictated by the balance of interfacial energies (γ_{SS} , γ_{SM}) about their line of intersection, and is given by equation 1 in the text.

Experiments were performed at a temperature of 1300°C, $f(O_2)$ of $10^{-8.1}$, $10^{-8.8}$ and $10^{-9.5}$, and nearly constant $f(S_2)$ of $10^{-1.75 \pm 0.15}$ (Table 1). Note that there is a small shift in $f(O_2)$ and $f(S_2)$ values listed in Table 1, compared to those provided in Rose & Brenan (2001). This is the result of a small change in the flow-rate calibration and an error in the input data (JANAF tables) for the free energy of formation (G_f) of the gas species S_2O , H_2S_2 and HS (V. Kress, pers. commun., 2001) used in these previous calculations. A revised version of the program COHSmix, kindly supplied by Victor Kress, was used to calculate the values of $f(O_2)$ and $f(S_2)$ in this paper. The accuracy of quoted sulfur fugacity was assessed using 1) the pyrrhotite sulfur barometer of Toulmin & Barton (1964) at 900°C and $\log f(S_2)$ of -1.5 , -2 and -3 , and 2) by determining the $f(S_2)$ of the Ru–RuS₂ equilibrium at 1200°C. Oxygen fugacity was checked using the stability of solid oxide buffers (nickel – nickel oxide, molybdenum – molybdenum oxide, iron–wüstite), and we have also employed the NiO–Pd redox sensor at 1000°C (Pownceby & O’Neill 1994). On the basis of this assessment, we estimate the accuracy in $f(S_2)$ and $f(O_2)$ to be within 0.3 log units.

Sulfide melt was added to experiments as mixtures of pure metal and elemental sulfur, weighed and ground to the desired proportions. A typical experiment contained this metal–sulfur mix (hereafter referred to as sulfide melt), powdered chromite from New Caledonia

(supplied by the Royal Ontario Museum; catalogue number M36331), and in most cases, powdered San Carlos olivine, packed in alternating layers within crucibles fabricated from San Carlos olivine megacrysts. In some samples, sulfide melt was “premixed” with separate chromite and olivine powders prior to packing into layers (*i.e.*, samples Cu5, Cu9a, b, c, and Co5), whereas other samples were prepared by packing discrete sulfide melt, chromite, \pm olivine layers into the olivine crucible. The main impetus for these separate packing arrangements was to allow individual chromite–melt and olivine–melt wetting angles to be measured from the products of a single experiment. A detailed account of the experimental technique employed in this study and specific results for olivine-bearing layers is documented in Rose & Brenan (2001).

Run products were mounted, polished, and carbon-coated in preparation for textural and electron-microprobe analyses. Run-product phases were analyzed using the JEOL JXA–8600 microprobe at the University of Western Ontario and the Cameca SX50 at the University of Toronto. Analyses were conducted using an accelerating voltage of 20 kV, a beam current of 30 nA, with on-peak counting times of 30 seconds. The analysis of sulfide melt used pentlandite (Fe, S, Ni), chalcopyrite (Cu), cobaltite (Co), hematite (O), and chromite (Cr) standards. Oxygen X-ray intensities were collected using an ODPB pseudocrystal, and the hema-

tite standard was carbon-coated at the same time as the unknowns to minimize inaccuracies due to the effects of coating thickness on attenuation of oxygen X-rays. Depending on the size of sulfide-melt pockets, a defocused beam of between 5 and 10 μm was used for analysis. We used gahnite (Al), MgO (Mg), MnTiO₃

(Mn, Ti), hematite (Fe), pentlandite (Ni), cobaltite (Co), Cu₂O (Cu), and Cr₂O₃ (Cr) as standards for chromite analyses. Raw count-rates were converted to concentrations using a modified ZAF correction routine. Summaries of measured sulfide liquid and representative compositions of chromite are provided in Tables 1 and 2, respectively.

TABLE 1. SUMMARY OF EXPERIMENTAL CONDITIONS AND SULFIDE MELT COMPOSITIONS

Sample	t hrs	log f(O ₂)	log f(S ₂)	Gas-flow rates CO:SO ₂ :CO ₂	Initial melt composition	n	Fe	Cu, Co, Ni	S	O	Cr	Total
FeS1	72	-8.8	-1.7	48 : 12 : 93	70-0-30	12	62.24 (1.25)	n.a.	28.82 (0.91)	7.39 (1.26)	1.84 (0.30)	100.29
Cu2	71	-8.8	-1.7	48 : 12 : 93	65-5-30	12	56.78 (2.65)	6.77 (2.50)	30.06 (2.42)	4.73 (1.53)	2.31 (0.52)	100.65
Cu5	72	-8.8	-1.7	48 : 12 : 93	40-30-30	11	42.27 (4.21)	23.00 (4.89)	29.25 (0.99)	4.06 (0.82)	1.82 (0.79)	100.40
Cu8	71	-8.8	-1.7	48 : 12 : 93	55-15-30	12	45.45 (2.60)	19.65 (3.21)	30.35 (0.90)	3.20 (0.72)	1.69 (0.32)	100.34
Cu9C	24	-9.5	-1.6	66 : 8 : 53	55-15-30	10	52.65 (2.49)	10.02 (2.25)	33.23 (1.17)	2.35 (0.88)	2.16 (0.73)	100.41
Cu9A	96	-9.5	-1.6	66 : 8 : 53	55-15-30	11	51.75 (3.24)	11.44 (4.06)	33.59 (1.21)	1.68 (0.58)	1.48 (0.39)	99.94
Cu9B	168	-9.5	-1.6	66 : 8 : 53	55-15-30	10	52.92 (2.20)	9.26 (2.28)	33.65 (0.89)	2.51 (0.67)	1.91 (0.43)	100.25
Co2	72	-8.8	-1.7	48 : 12 : 93	65-5-30	11	58.21 (0.65)	4.79 (0.24)	30.99 (1.25)	4.62 (1.26)	2.14 (0.34)	100.75
Co5	73	-8.8	-1.7	48 : 12 : 93	40-30-30	13	33.92 (3.64)	29.93 (4.34)	33.09 (1.31)	1.60 (1.15)	1.64 (0.49)	100.18
Ni2A	72	-8.8	-1.7	48 : 12 : 93	65-5-30	16	59.47 (2.55)	5.67 (2.07)	29.43 (2.44)	4.94 (2.02)	1.34 (0.27)	100.85
Ni2B	120	-8.8	-1.7	48 : 12 : 93	65-5-30	28	57.49 (1.53)	8.27 (2.09)	30.36 (1.49)	2.98 (1.34)	1.52 (0.31)	100.62
Ni2C	168	-8.8	-1.7	48 : 12 : 93	65-5-30	10	59.48 (1.87)	5.31 (1.70)	29.86 (2.11)	3.92 (1.81)	1.50 (0.50)	100.07
Ni4B	120	-8.8	-1.7	48 : 12 : 93	55-15-30	22	47.78 (3.20)	18.84 (3.90)	30.38 (0.80)	2.02 (1.12)	1.15 (0.41)	100.17
Ni4C	168	-8.8	-1.7	48 : 12 : 93	55-15-30	12	49.75 (2.46)	16.19 (2.63)	30.71 (0.87)	2.41 (0.82)	1.63 (0.76)	100.69
Ni5A	72	-8.8	-1.7	48 : 12 : 93	45-25-30	20	38.05 (2.05)	29.18 (2.72)	30.93 (0.74)	<0.20	0.92 (0.32)	99.08
Ni5B	120	-8.8	-1.7	48 : 12 : 93	45-25-30	13	38.81 (2.40)	27.13 (2.64)	31.45 (0.69)	0.27 (0.33)	2.05 (0.39)	99.71
Ni5C	168	-8.8	-1.7	48 : 12 : 93	45-25-30	13	38.70 (2.35)	28.86 (3.87)	31.05 (1.38)	0.23 (0.57)	1.48 (0.56)	100.32
Ni7	120	-9.5	-1.6	66 : 8 : 53	65-5-30	19	57.95 (1.18)	5.00 (1.42)	33.93 (0.90)	0.92 (0.84)	2.61 (0.62)	100.41
Ni12B	85	-8.1	-1.9	25 : 27 : 96	45-25-30	16	21.25 (2.06)	48.89 (3.14)	27.48 (1.53)	0.70 (0.81)	1.86 (0.62)	100.18

All experiments were performed at 1300°C. Melt compositions are based on multiple broad-beam electron-microprobe analyses. All samples contain chemically isolated olivine and chromite layers except samples Ni2A, Ni5A, and Ni12B, which contain a single chromite layer only. Numbers in parentheses refers to the error based on one standard deviation of results of *n* analyses. The gas-flow rates are quoted in cm³ per minute. The initial composition of the melt (e.g., 70-0-30) is expressed in the order Fe-(Cu,Co,Ni)-S (wt%).

TABLE 2. REPRESENTATIVE COMPOSITIONS OF CHROMITE RIM IN CONTACT WITH SULFIDE MELT

Sample	t hrs	log f(O ₂)	log f(S ₂)	Ni wt% sulfide L	n	MgO	Al ₂ O ₃	MnO	FeO	NiO	Cr ₂ O ₃	TiO ₂	Total
M36331					15	16.17 (0.14)	10.78 (0.11)	—	13.57 (0.29)	—	58.58 (0.57)	0.12 (0.01)	99.22
Ni2A	72	-8.8	-1.7	5.67 (2.07)	27	12.28 (0.22)	11.44 (0.86)	0.02 (0.01)	22.31 (1.37)	0.07 (0.03)	52.60 (2.91)	0.2 (0.05)	98.92
Ni2B	120	-8.8	-1.7	8.27 (2.09)	15	11.51 (0.15)	14.78 (0.36)	0.01 (0.01)	24.25 (0.46)	0.09 (0.04)	47.87 (0.71)	0.13 (0.02)	98.64
Ni2C	168	-8.8	-1.7	5.31 (1.70)	15	13.19 (0.28)	10.72 (0.52)	0.01 (0.01)	22.78 (1.13)	0.06 (0.02)	51.48 (1.12)	0.13 (0.02)	98.37
Ni7	120	-9.5	-1.6	5.00 (1.42)	21	13.47 (0.35)	15.07 (0.85)	0.01 (0.01)	15.64 (0.79)	0.07 (0.06)	54.32 (1.66)	0.13 (0.02)	98.71
Ni12B	85	-8.1	-1.9	48.89 (3.14)	13	10.39 (0.43)	8.13 (0.49)	0.01 (0.02)	28.01 (4.30)	0.81 (0.21)	51.03 (5.09)	0.08 (0.01)	98.46
Ni4B	120	-8.8	-1.7	18.84 (3.90)	23	11.42 (0.25)	14.38 (0.98)	0.01 (0.01)	23.95 (1.49)	0.24 (0.15)	48.67 (2.12)	0.16 (0.03)	98.83
Ni5B	120	-8.8	-1.7	27.13 (2.64)	9	11.73 (0.51)	14.32 (3.11)	0.06 (0.02)	20.69 (0.30)	0.45 (0.08)	51.96 (3.72)	0.14 (0.02)	99.34

M36331 is the chromite starting material. Compositions expressed in wt%. Numbers in parentheses refers to the error based on one standard deviation of results of *n* analyses.

For any random section through a sample characterized by a single dihedral angle, a distribution of "apparent" angles is expected, as the plane of the section cuts triple junctions that are randomly oriented with respect to the acute bisectrix of the true dihedral angle. Harker & Parker (1945) showed, however, that the median value of a range of apparent measured angles represents the true dihedral angle. As such, we measured approximately 100 angles for each sample using digitized back-scattered electron (BSE) images taken at magnifications of approximately 1000 to 2000 \times . All dihedral angles exposed on a given image were measured. The associated uncertainty in the dihedral angle determined in this way was calculated using the method of Riegger & Van Vlack (1960). On the basis of replicate measurements, the error associated with a single measurement was found to be $\pm 2^\circ$. The chromite - sulfide melt system behaves anisotropically with respect to surface energy, as between 10 and 15% of the chromite grains produced in this study display crystal facets (Fig. 2). Dihedral angles involving such interfaces were not included in the median value, as their effect on the permeability of the matrix has not been well established. Waff & Faul (1992) argued that the presence of facets serves to *increase* matrix permeability by reducing the occurrence of "pinch-off" along grain edge intersections. In contrast, in their study monitoring bulk diffusion in fluid-bearing aggregates of pyroxene, Watson & Lupulescu (1993) determined that the median dihedral angle involving only curved interfaces was a reliable predictor of permeability, despite the presence of abundant faceted interfaces. A summary of values of the dihedral angle is provided in Table 3.

TABLE 3. DIHEDRAL ANGLE MEASURED BETWEEN CHROMITE AND SULFIDE LIQUID

Sample	<i>n</i> ^a	Dihedral Angle ^b	Sample	<i>n</i> ^a	Dihedral Angle ^b
FeS1	141	41 (1)	Ni2A	96	42 (2)
Cu2	153	40 (1)	Ni2B	97	44 (2)
Cu5	127	52 (2)	Ni2C	110	41 (2)
Cu8	115	53 (2)	Ni4B	101	47 (2)
Cu9c	110	65 (2)	Ni4C	106	46 (2)
Cu9a	101	64 (3)	Ni5A	109	53 (2)
Cu9b	100	64 (3)	Ni5B	80	53 (2)
Co2	77	44 (2)	Ni5C	98	53 (2)
Co5	71	60 (3)	Ni7	102	53 (2)
			Ni12B	106	53 (2)

a) number of measured dihedral angles included in calculation of the median value.
b) number in parentheses refers to the error based on one standard deviation of *n* angles as derived by Riegger & Van Vlack (1960).

RESULTS AND DISCUSSION

Overview

Run products consisted of solid layers containing chromite or olivine, both with interstitial sulfide liquid. In "layered" experiments where melt and solid layers were packed separately, melts migrated from their initial position between the packed mineral layers, leaving significant interlayer void space behind. This resulted in "suspended" melt-impregnated layers, attached on each end to the crucible walls. In "premixed" experiments, where melt and solid were mixed prior to sample assembly, discrete melt-bearing olivine and chromite layers still resulted, yet were separated by a much thinner interlayer void space. Examples of the textural

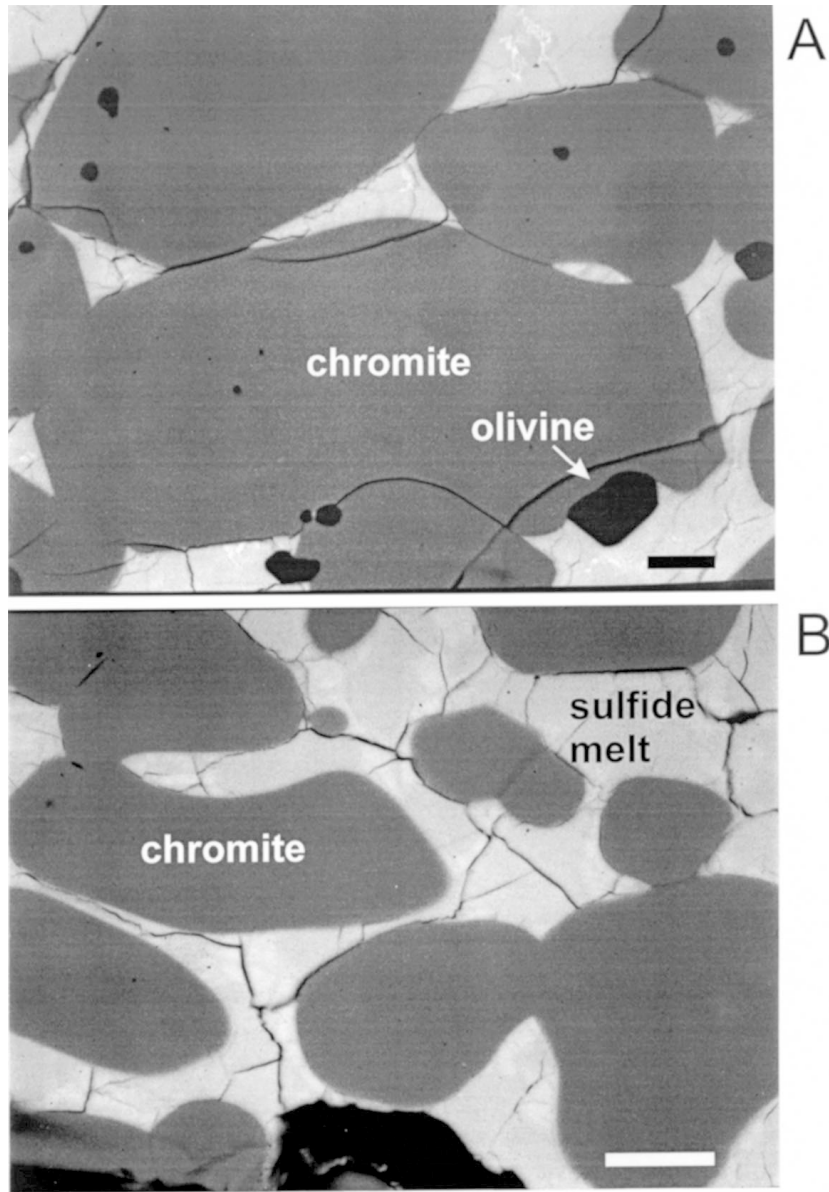


FIG. 2. Back-scattered electron images of sectioned run-products consisting of sulfide melt, chromite and minor olivine. A) and B) contrast the textures produced in experiments Ni2c and Cu9a, in which median dihedral angles are 41° and 64° , respectively. Scale bars represent $10\ \mu\text{m}$.

development of run-products are provided in Figure 2. In this case, samples exhibiting values of θ both below (41° , Fig. 2A) and above (64° , Fig. 2B) the critical value of 60° are shown. The most distinctive contrast in tex-

ture between these samples is that at chromite – chromite – melt junctions, most grain faces are convex toward the melt in Figure 2A, whereas they are concave in Figure 2B.

Phase chemistry

Sulfide melts produced in our experiments consisted mainly of Fe (21–62 wt%), S (27–34 wt%) and either Ni, Cu, or Co (4–49 wt%), in addition to varying amounts of oxygen [0–7 wt%, depending on $f(\text{O}_2)$ and the identity of added non-ferrous metals], and Cr (1–2.5 wt%) (Table 1). The relatively large standard deviation in inferred oxygen contents of the melt is a consequence of the difficulties in analyzing for this element in melts with abundant quench phases. Moreover, the melt pockets produced in our experiments are relatively small, and melt compositions may, in some cases, be compromised by impingement of the electron beam on adjacent chromite, an oxygen-rich phase. Chromite grains produced in this study exhibit homogeneous overgrowths that are generally enriched in Fe and deficient in Cr and Mg relative to the residual starting material. Detailed analyses of overgrowths from experiments containing nickel-bearing sulfide melt (Table 2) revealed an excellent correlation between Ni concentration of chromite and melt (Fig. 3A; $r = 0.997$ forced through the origin), indicating adherence to Henry's Law for chromite–melt partitioning. Moreover, the calculated ferric iron content of chromite from those experiments shifted with both melt Fe content and imposed oxygen fugacity (Fig. 3B). Reconnaissance analyses of chromite rims from runs containing cobalt- and copper-bearing sulfide melt revealed significant uptake of cobalt (~3 wt%) relative to either copper (~0.2 wt%) or nickel (~0.4 wt%) for melts with similar total concentrations of these elements (20–30 wt%). The systematic variation in compositions of the chromite overgrowth with melt composition and $f(\text{O}_2)$ suggests that the overgrowths formed by dissolution and reprecipitation during equilibration with the surrounding sulfide melt at the specific conditions of $f(\text{O}_2)$ and $f(\text{S}_2)$. A comparison between compositions of the chromite rim produced in this study with those from a variety of natural parageneses is provided in Figure 4. The chromite produced in this study is characterized by low Al and Fe^{3+} , similar to chromite from stratiform intrusions and ophiolites (see also Barnes & Roeder 2001).

Dihedral angles between chromite and sulfide melt

To test whether textural equilibrium has been achieved, three sets of time-series experiments were conducted at constant $f(\text{O}_2)$, $f(\text{S}_2)$, and initial melt composition. The Cu9 series of experiments was conducted at an $f(\text{O}_2)$ of $10^{-9.5}$; they contained 15 wt% Ni in the initial sulfide melt, and ran for durations of 24, 96, and 168 hours. As shown in Figure 5, dihedral angles were found to be constant with experiment duration, suggesting that textural equilibrium was attained in runs as short as 24 hours. Similar results were obtained for the Ni2, Ni4, and Ni5 time series, which were conducted at an $f(\text{O}_2)$ of $10^{-8.8}$, and contained 5, 15, and 25 wt% Ni, re-

spectively, in the initial sulfide melt. Given these results, an experimental duration of 72 hours was considered sufficient for textural equilibrium, and was therefore chosen for all other experiments.

Dihedral angles between chromite and sulfide melt determined from our experiments ranged from 40° to 65° (Table 3). Values of θ become larger with increases in abundance of non-ferrous metal in the melt or decreasing $f(\text{O}_2)$ (Fig. 6). For example, at an $f(\text{O}_2)$ of $10^{-8.8}$, an increase in the nickel abundance of melt from 5.7 to 29.2 wt% results in an increase in the measured dihedral angle from 42° to 53° . Similar effects were observed with the addition of Cu and Co to the sulfide

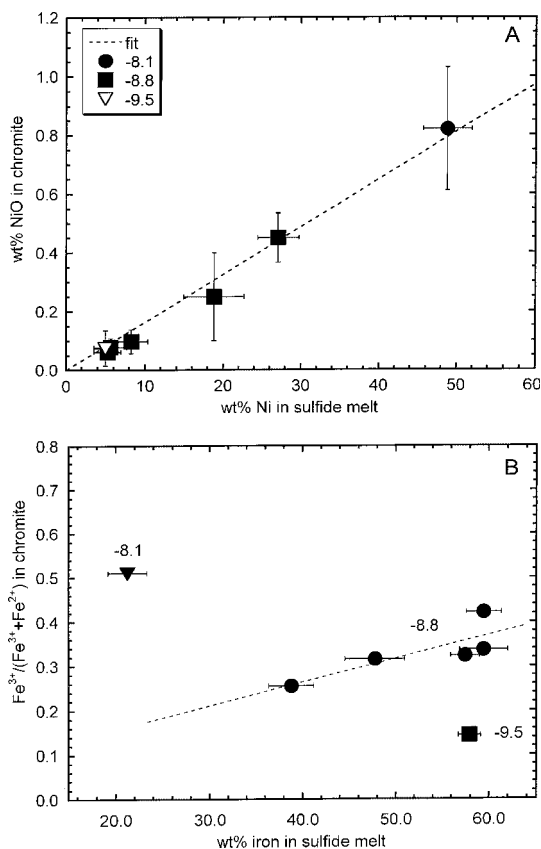


Fig. 3. A) Variation in the NiO abundance in chromite as a function of the Ni content of coexisting sulfide melt. Experiments were conducted at the log $f(\text{O}_2)$ values indicated in the legend. The dashed line is a linear regression through all the data, and is constrained to include the origin ($r = 0.997$). B) Variation in the ratio of ferric iron to total iron in the chromite as a function of the iron content of the sulfide melt. Experiments are labeled according to the imposed log $f(\text{O}_2)$. The dashed curve is a linear regression of the data at log $f(\text{O}_2)$ of -8.8 ($r = 0.803$).

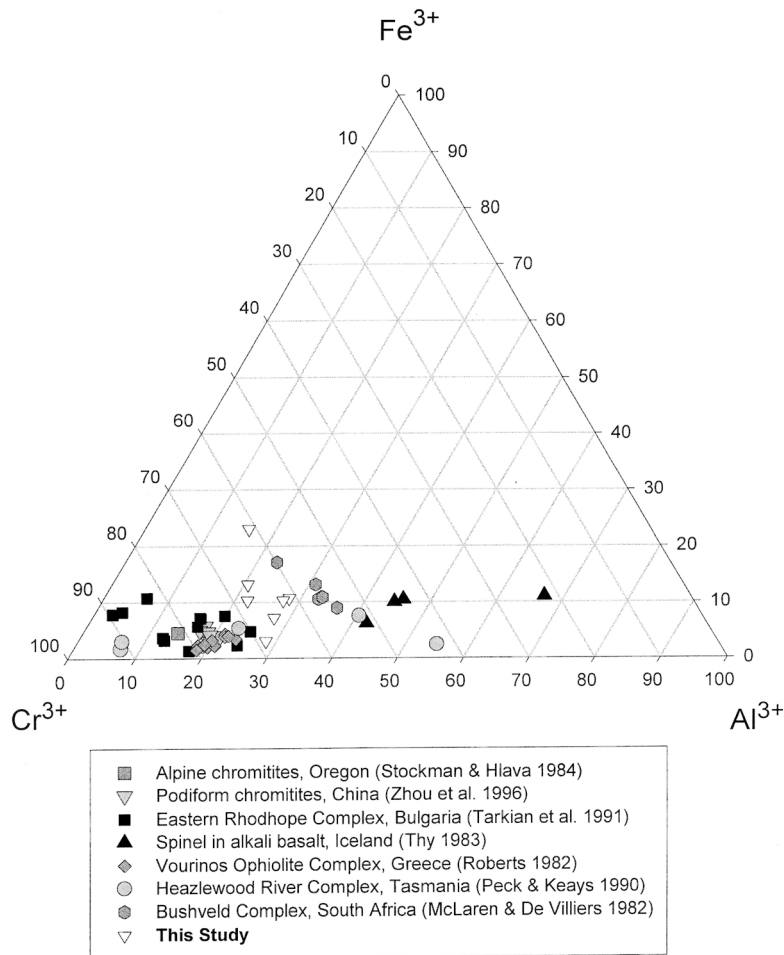


FIG. 4. Plot depicting chromite compositions (trivalent cation %) produced in this study in comparison to chromite from various geological settings.

melt. At a given $f(O_2)$, $f(S_2)$ and melt composition, values of θ for chromite – sulfide melt are lower ($\sim 13^\circ$ on average) than those we previously determined for olivine (Rose & Brenan 2001), as seen in Figure 7. For example, in the “control” sample (FeS1, containing only Fe–S–O), a dihedral angle of 58° was determined from olivine-bearing layers, whereas a value of 41.5° was measured for those containing chromite. Inasmuch as melt connectivity is enhanced as the value of θ decreases (*e.g.*, Von Bargen & Waff 1986), the relative difference in dihedral angles for olivine and chromite suggests that the permeabilities of rocks dominated by either of these minerals will vary likewise, with sulfide-melt-bearing olivine-rich lithologies being less permeable than those rich in chromite.

Variation of θ with melt composition

As discussed in Rose & Brenan (2001), variation in the olivine – sulfide melt dihedral angle with the non-ferrous metal content of the melt can be attributed to changes in the solid–liquid interfacial energy stemming from differences in the abundance of surface-active species within the melt. Results from olivine – sulfide melt wetting experiments suggest that the main surface-active component is likely to be an Fe-oxide species ($Fe_{1-x}O$), on the basis of well-defined correlations between the Fe or oxygen content of the melt, and θ (Gaetani & Grove 1999, Rose & Brenan 2001). Thus, the preferential adsorption of this species results in an overall reduction in γ_{SM} , which consequently lowers θ , as defined in equa-

tion 1. As shown in Figure 8, the oxygen content of the sulfide melts produced in this study is positively correlated with the iron content of the melt, suggesting that the dominant oxide species in these mixed-metal melts

is also Fe-bearing. Cobalt- and copper-rich sulfide liquids appear to have higher oxygen contents compared to those containing nickel (at a given Fe content in the melt), however, which may indicate that oxygen also

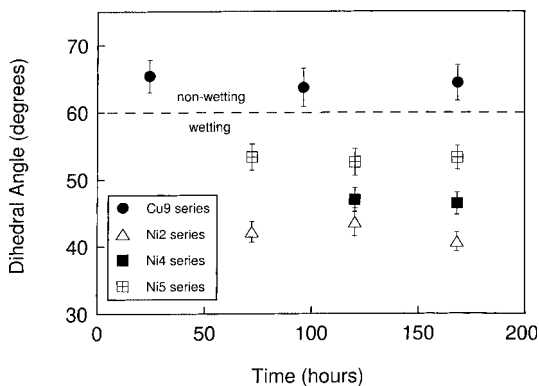


FIG. 5. Variation in dihedral angle between chromite and sulfide melt as a function of run duration for Cu- and Ni-doped experiments produced at an $f(O_2)$ of $10^{-9.5}$ and $10^{-8.8}$, respectively. The data illustrate the invariance of the dihedral angle with time. The error associated with the measurement of the dihedral angle is based on one standard deviation of n measured "apparent" angles (Riegger & Van Vlack 1960).

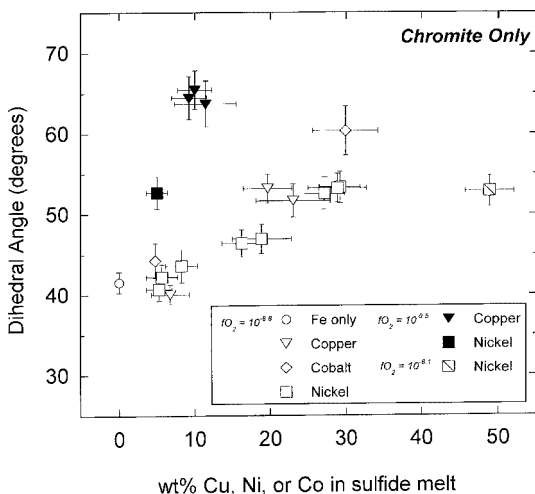


FIG. 6. Variation in dihedral angle between chromite and sulfide melt as a function of the amount (wt%) of non-ferrous transition metal in the sulfide melt. Results are shown for samples produced in this study at $f(O_2)$ values of $10^{-8.1}$, $10^{-8.8}$ and $10^{-9.5}$. Measured values of θ increase as the amount of added metal increases, regardless of metal identity.

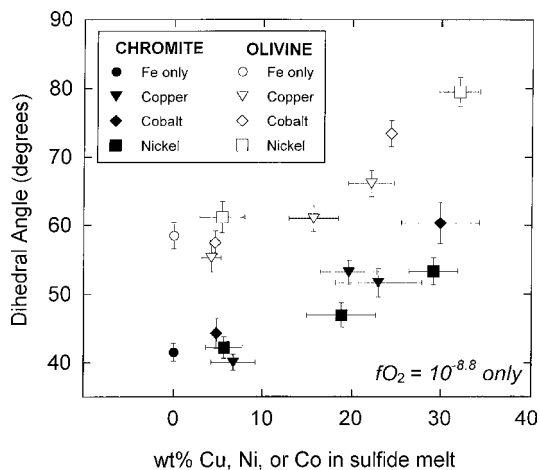


FIG. 7. Comparison of dihedral angles between chromite and sulfide melt with those for olivine (Rose & Brenan 2001), at $f(O_2) = 10^{-8.8}$ and over the same range of melt composition. Measured dihedral angles are on average $\sim 13^\circ$ lower for chromite than for olivine. The error on metal content of the melt is based on one standard deviation of n analyses.

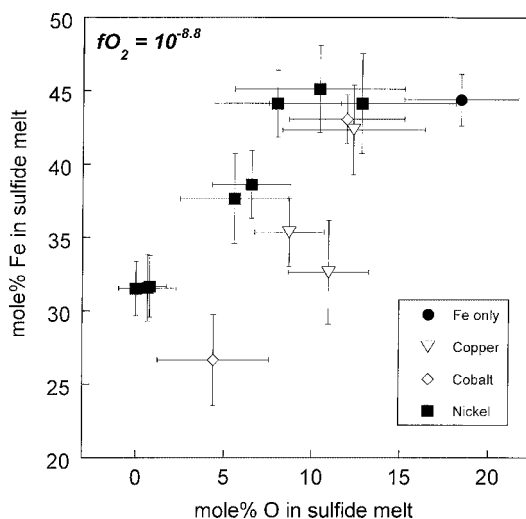


FIG. 8. Variation in mole % oxygen as a function of mole % iron for sulfide liquids produced at $f(O_2) = 10^{-8.8}$. An increase in the amount of Fe within the sulfide liquid is also reflected in an increase in the amount of O, suggesting that oxygen dissolves in the melt as an iron oxide species.

dissolves as Co- and Cu-bearing species in such melts. To determine whether a dissolved iron-oxide species is important in controlling the chromite–melt wetting behavior, we have plotted θ as a function of the mole % oxygen in the sulfide liquid at a constant $f(\text{O}_2)$ of $10^{-8.8}$, and results are portrayed in Figure 9. As in the case for olivine, an increase in dissolved oxygen within the melt produces a decrease in the dihedral angle between chromite and sulfide melt. Melts with elevated Co or Cu contents appear to produce dihedral angles that are systematically larger than nickel-bearing melts, at the same dissolved oxygen content. The abundance of surface-active Fe-oxide species thus seems lower in such melts, as a consequence of the sequestering of oxygen by surface-“inert” cobalt- and copper-bearing species.

An unambiguous assessment of the mechanism responsible for the observed variation in θ is made difficult, however, by the fact that the composition of the chromite produced in experiments varies with both melt Fe content (and hence O content) and $f(\text{O}_2)$. Thus, in addition to the effect of melt composition on γ_{SM} , changes in chromite composition could affect either γ_{SS} or γ_{SM} , thus obviating the need to call upon surface adsorption as a mechanism for changes in dihedral angle. A systematic search for the chromite compositional parameter that produces a significant correlation with θ reveals that the ferric iron content of the chromite is best correlated ($r = 0.886$; Fig. 10A), with θ decreasing with increasing ferric iron in chromite produced from Ni-bearing melts at $f(\text{O}_2)$ of $10^{-8.8}$. The data for chromite produced at $f(\text{O}_2)$ of $10^{-8.1}$ and $10^{-9.5}$ are offset from this trend, however, and reveal higher and lower ferric

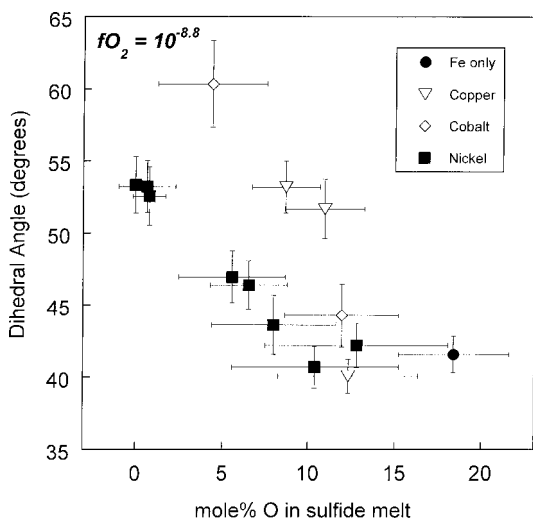


FIG. 9. Variation in the dihedral angle between chromite and sulfide melt with oxygen content in the melt (mole %) for sulfide liquids produced at $f(\text{O}_2) = 10^{-8.8}$.

iron contents, respectively, for a given value of θ . Thus although an increase in ferric iron seems to result in a relative increase in $\gamma_{\text{SS}}/\gamma_{\text{SM}}$, this result only applies to a specific $f(\text{O}_2)$. A notable aspect of Figure 10A is that the experiments that produced the largest dihedral angles all contain melts with the lowest oxygen contents. As shown in Figure 10B, a single, $f(\text{O}_2)$ -independent correlation exists between θ and oxygen content of melt for all of these experiments. In this context, the correlation between ferric iron content of the chromite and θ is simply a consequence of the former value increasing with melt Fe and O concentration. We conclude that, as is the case for olivine, the variation in chromite–melt

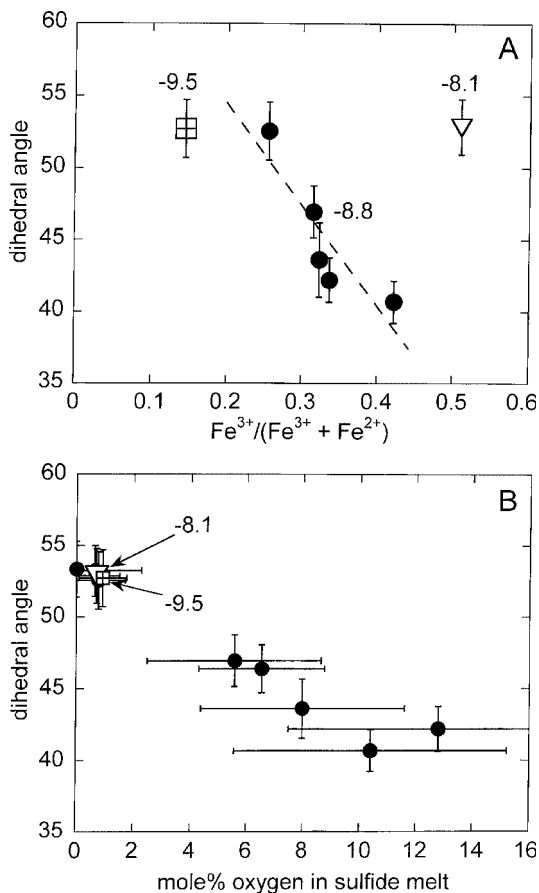


FIG. 10. A) Variation in the dihedral angle between chromite and sulfide melt as a function of the ratio of ferric iron to total iron in chromite coexisting with Ni-bearing sulfide melt [the data are labeled according to experimental $\log f(\text{O}_2)$]. The dashed curve through the data at a $\log f(\text{O}_2)$ of -8.8 is a linear regression of the data ($r = 0.886$). B) Variation in dihedral angle between chromite and sulfide melt as a function of melt oxygen content (same dataset as plotted in 10A).

dihedral angle with melt composition is most consistent with a melt composition effect, with the adsorption of an iron-oxide species in the melt being the likely mechanism for the reduction in θ .

Implications for sulfide distribution in chromitites

Significantly, the majority of our experiments produced dihedral angles between chromite and sulfide melt of less than 60° , and those that did not were either extraordinarily rich in cobalt (~30 wt%; Co5) or were Cu-rich and run at the lowest $f(\text{O}_2)$ (~10 wt%; Cu9a,b,c). Inasmuch as most mafic magmas record values of $f(\text{O}_2)$ at or above those of our experiments, (e.g., Wallace & Carmichael 1993), and produce sulfide liquids with generally less extreme abundances of non-ferrous metal, our results suggest that natural sulfide liquids are quite likely to be “wetting” against chromite. Assessment of the overall permeability of natural chromitites requires, however, some information on the wettability of interfaces involving chromite and the accessory silicate minerals likely to be present in such rocks (*i.e.*, olivine, orthopyroxene, plagioclase). As a consequence of using olivine as an encapsulating material, all chromite layers from our experiments contain small, euhedral grains of olivine. Observations of the chromite–olivine contact relations in these experiments yield information on the relative wetting properties of both these minerals with respect to sulfide liquid, and allow us to partially address the effect of silicate mineral “impurities” on rock permeability. In experiments that produced the lowest dihedral angles [FeS1 and those with melts having the highest Fe contents done at $\log f(\text{O}_2)$ of -8.8], we observed triple junctions formed at the intersection between two grains of chromite and an olivine grain that were both “wet” (*i.e.*, melt-bearing) and “dry” (*i.e.*, melt-free) within the same sample (Fig. 11). Experiments at lower $f(\text{O}_2)$ or with melts having lower Fe concentrations showed only “dry” chromite–olivine triple junctions. The latter observation of dual wetting behavior is likely to be the result of anisotropy in the surface energies of olivine and chromite, since even small differences in either γ_{SS} or γ_{SM} can have a large effect on θ (eq. 1). The occurrence of melt-free chromite–olivine triple junctions indicates that the olivine–chromite interface has a lower free energy than that in contact with sulfide liquid. The presence of accessory olivine (and possibly other silicate minerals) thus could serve to truncate melt-filled tubules occupying chromite grain-edges, reducing melt connectivity and the permeability of natural chromitites. This effect is $f(\text{O}_2)$ - and melt-composition-dependent, however, as melt-bearing interfaces become dry in the more oxygen- and iron-poor melt composition investigated, which also yielded uniformly higher values of θ . At higher $f(\text{O}_2)$, there may be a greater range of liquid compositions that result in wetted chromite–olivine interfaces, thus enhancing melt connectivity.

In addition to implications for the connectivity of the melt phase, values of θ also provide an indication of the possibility of melt migration driven by variations in surface energy. As shown by Watson (1982), values of θ less than 60° for a particular melt–mineral pair indicate that a given area of melt–mineral interface is at a lower energy than the equivalent area of mineral–mineral interface. As a consequence, melt will migrate into a region containing “dry” mineral–mineral interfaces in order to reduce the total surface-energy of the system. This process of infiltration will occur at chemical equilibrium, and in the *absence* of any external driving force, such as temperature or pressure gradients, but must involve local dissolution–reprecipitation of the host-rock mineral constituents (Watson 1982). Given the low values of θ measured for the chromite–sulfide system over a range in $f(\text{O}_2)$ and melt composition, it is plausible that natural chromitites could be susceptible to infiltration metasomatism by sulfide liquid, and such a process is most likely to arise if sulfide saturation immediately pre- or postdates chromite segregation. Thus, the presence of interstitial base-metal sulfides in chromitites may not require sulfide saturation to occur simultaneously with chromite crystallization, as might be concluded from textural relations alone. Infiltration of sulfide liquid would clearly serve to enhance the Ni, Cu and PGE tenor of chromitite horizons, as these components are far more concentrated in molten sulfide than in chromite, or associated silicate minerals (*cf.* Sattari *et al.* 2002). Moreover, postcumulus infiltration of molten sulfide may also explain the conspicuous absence of interstitial (IPGE)-rich accessory minerals, *i.e.*, those enriched in Ru, Os and Ir, such as laurite (RuS_2), in chromitites containing such phases as intracrystalline inclusions. For example, Maier *et al.* (1999) conducted a survey of the compositional variation in laurite from the Western Bushveld Complex, and found that 91% were present as inclusions in chromite, with 7% located at silicate mineral – chromite grain boundaries, 1.5% as inclusions in silicate minerals, with a single grain included in base-metal sulfide. Recent experiments have shown that the solubility of Ru-rich phases in molten sulfide is far too high for them to crystallize at the levels of Ru present in natural sulfide liquids (Brenan & Andrews 2001, Andrews & Brenan 2002). Thus, if such phases form early in the crystallization sequence of chromitites, as suggested by textural relations, then they must predate sulfide saturation. Infiltration of later-formed sulfide melt would serve to dissolve early-formed laurite present as an interstitial phase, preserving only those grains that were either a) shielded by a mineral host, b) occurring along grain contacts unfavorable to sulfide penetration (*i.e.* silicate mineral – chromite), or c) incompletely dissolved owing to sluggish dissolution kinetics. Any Ru–Os–Ir-bearing accessory minerals associated with interstitial sulfide could also be the result of subsolidus exsolution from base-metal sulfides due to reduced solubility in these phases with decreas-

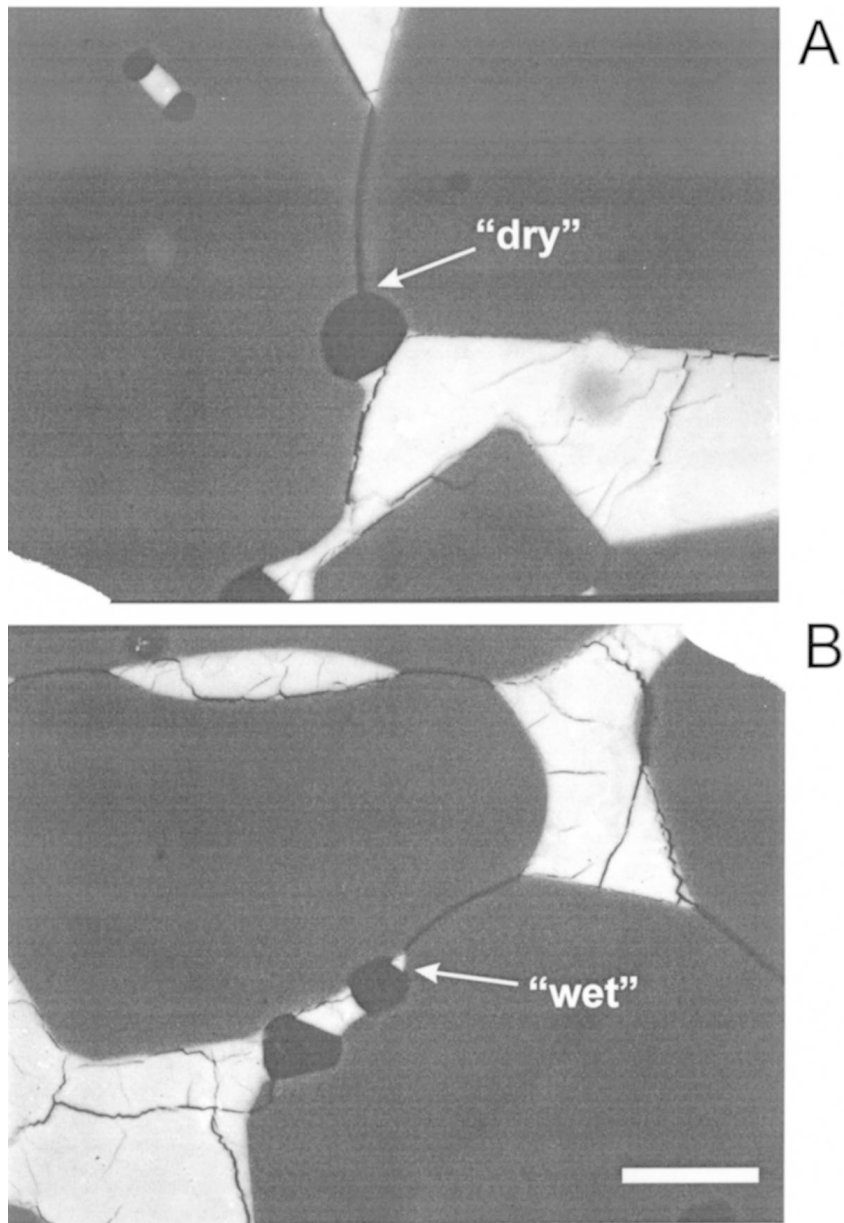


FIG. 11. Back-scattered electron images of sectioned run-products from experiment Ni2c, consisting of sulfide melt, chromite and minor olivine. A) and B) show examples of triple junctions between two chromite crystals and olivine that are "dry" (sulfide-melt-free) and "wet" (sulfide-melt-bearing). Scale bar represents 10 μm .

ing temperature (e.g., Ballhaus & Ulmer 1995, Brenan *et al.* 2000). The magmatic origin of the interstitial base-metal sulfide in the Bushveld chromitites is clearly demonstrated by the near-chondritic osmium isotopic composition of this phase, and its similarity in isotopic composition to coexisting chromite (e.g., Schoenberg *et al.* 1999).

CONCLUSIONS

We have found that wetting angles between chromite and sulfide melt are less than 60° over a wide range of melt compositions and at $f(\text{O}_2)$ relevant to the generation of terrestrial magmas. Values of θ are uniformly lower ($\sim 13^\circ$) for chromite than those we have previously determined for olivine over a similar range of conditions. Dihedral angles between chromite and sulfide melt decrease with increasing oxygen and iron in the sulfide melt. This relation is defined by a single, $f(\text{O}_2)$ -independent correlation, suggesting that the variation in θ is related to absorption of an Fe-oxide species, as previously suggested for olivine (Gaetani & Grove 1999, Rose & Brenan 2001). Low values of θ indicate that sulfide melts in chromite-rich rocks are likely to be interconnected, thus allowing melt migration to occur by porous flow, and indicating that chromitite horizons in ophiolites and stratiform intrusions will not impede the redistribution of sulfide melt between layers. Infiltration metasomatism of chromitites from adjacent sulfide-melt-rich domains is also possible, and may serve to locally enhance chromitite tenor, and dissolve any interstitial IPGE-rich accessory minerals that precipitated initially with the chromite.

ACKNOWLEDGEMENTS

We thank Claudio Cermignani (University of Toronto) and Yves Thibault (formerly at the University of Western Ontario) for their help with the electron-microprobe analyses. We are grateful to Bob Ramik of The Royal Ontario Museum for generously supplying the New Caledonia chromite sample to JMB. Dave Andrews is thanked for his endless supply of fused quartz sample holders. Reviews by Steve Barnes and an anonymous referee helped to improve the clarity of presentation, as did the skillful editing of R.F. Martin. Research was supported by NSERC operating grant OGP 0194228 to JMB, and LAR received scholarship support from the University of Toronto.

REFERENCES

- ANDREWS, D.A. & BRENNAN, J.M. (2002): The solubility of ruthenium in sulphide liquid: implications for platinum-group mineral (PGM) stability and sulphide melt/silicate melt partitioning. *Chem. Geol.*, in press.
- BALLHAUS, C. & ELLIS, D.J. (1996): Mobility of core melts during Earth's accretion. *Earth Planet. Sci. Lett.* **143**, 137-145.
- _____ & ULMER, P. (1995): Platinum-group elements in the Merensky Reef. II. Experimental solubilities of platinum and palladium in Fe_{1-x}S from 950 to 450°C under controlled $f\text{S}_2$ and $f\text{H}_2$. *Geochim. Cosmochim. Acta* **59**, 4881-4888.
- BARNES, S.J. & ROEDER, P.L. (2001): The range of spinel compositions in terrestrial mafic and ultramafic rocks. *J. Petrol.* **42**, 2279-2302.
- BRENNAN, J.M. & ANDREWS, D.A. (2001): High-temperature stability of laurite and Ru-Os-Ir alloy and their role in PGE fractionation in mafic magmas. *Can. Mineral.* **39**, 341-360.
- _____, CHERNIAK, D.J. & ROSE, L.A. (2000): Diffusion of osmium in pyrrhotite and pyrite: implications for closure of the Re-Os isotopic system. *Earth Planet. Sci. Lett.* **180**, 399-413.
- GAETANI, G.A. & GROVE, T.L. (1999): Wetting of mantle olivine by sulfide melt: implications for Re/Os ratios in mantle peridotite and late-stage core formation. *Earth Planet. Sci. Lett.* **169**, 147-163.
- HARKER, D. & PARKER, E.R. (1945): Grain shape and grain growth. *Trans. Am. Soc. Metals* **34**, 156-201.
- IRVINE, T.N. (1977): Origin of chromitite layers in the Muskog intrusion and other stratiform intrusions: a new interpretation. *Geology* **5**, 273-277.
- _____, KEITH, D.W. & TODD, S.G. (1983): The J-M platinum-palladium reef of the Stillwater Complex, Montana. II. Origin by double-diffusive convective magma mixing and implications for the Bushveld Complex. *Econ. Geol.* **78**, 1287-1334.
- JUREWICZ, S.R. & WATSON, E.B. (1984): Distribution of partial melt in a felsic system: the importance of surface energy. *Contrib. Mineral. Petrol.* **85**, 25-29.
- MAIER, W.D., PRICHARD, H.H., FISHER, P.C. & BARNES, S.-J. (1999): Compositional variation of laurite at Union Section in the Western Bushveld Complex. *S. Afr. J. Geol.* **102**, 286-292.
- McLAREN, C.H. & DE VILLIERS, J.P.R. (1982): The platinum-group chemistry and mineralogy of the UG-2 chromitite layer of the Bushveld Complex, *Econ. Geol.* **77**, 1348-1366.
- MERKLE, R.K. (1992): Platinum-group minerals in the middle group of chromitite layers at Marikana, western Bushveld Complex: indications for collection mechanisms and postmagmatic modification. *Can. J. Earth Sci.* **29**, 209-221.
- MINARIK, W.G., RYERSON, F.J. & WATSON, E.B. (1996): Textural entrapment of core-forming melts. *Science* **272**, 530-533.

- PECK, D.C. & KEAYS, R.R. (1990): Geology, geochemistry, and origin of platinum-group element – chromite occurrences in the Heazlewood River Complex, Tasmania. *Econ. Geol.* **85**, 765-793.
- POWNCEBY, M.I. & O'NEILL, H.St.C. (1994): Thermodynamic data from redox reactions at high temperatures. III. Activity–composition relations in Ni–Pd alloys from EMF measurements at 850–1250 K, and calibration of the NiO + Ni – Pd assemblage as a redox sensor. *Contrib. Mineral. Petrol.* **116**, 327-339.
- RIEGGER, O.K. & VAN VLACK, L.H. (1960): Dihedral angle measurement. *Trans. Metal. Soc. AIME* **218**, 933-935.
- ROBERTS, S. (1992): Influence of the partial melting regime on the formation of ophiolitic chromitite. In *Ophiolites and their Modern Oceanic Analogues* (L.M. Parson, B.J. Murton & P. Browning, eds.). *Geol. Soc., Spec. Publ.* **60**, 203-217.
- ROSE, L.A. & BRENNAN, J.M. (2001): Wetting properties of Fe–Ni–Cu–Co–O–S melts against olivine: implications for sulfide liquid mobility. *Econ. Geol.* **96**, 145-157.
- SATTARI, P., BRENNAN, J.M., HORN, I. & McDONOUGH, W.F. (2002): Experimental constraints on the sulfide– and chromite–silicate melt partitioning behavior of rhenium and platinum-group elements. *Econ. Geol.* **97**, 385-398.
- SCHOENBERG, R., KRUGER, F.J., NÄGLER, T.F., MEISEL, T. & KRAMERS, J.D. (1999): PGE enrichment in chromitite layers and the Merensky Reef of the western Bushveld Complex; a Re–Os and Rb–Sr isotope study. *Earth Planet. Sci. Lett.* **172**, 49-64.
- SHANNON, M.C. & AGEE, C.B. (1996): High pressure constraints on percolative core formation. *Geophys. Res. Lett.* **23**, 2717-2720.
- _____ & _____ (1998): Percolation of core melts at lower mantle conditions. *Science* **280**, 1059-1061.
- STOCKMAN, H.W. & HLAVA, P.F. (1984): Platinum-group minerals in Alpine chromitites from southwestern Oregon. *Econ. Geol.* **79**, 491-508.
- TARKIAN, M., NAIDENOVA, E. & ZHELIVSKOVA-PANAYOTOVA, M. (1991): Platinum-group minerals in chromitites from the eastern Rhodope ultramafic complex, Bulgaria. *Mineral. Petrol.* **44**, 73-87.
- THY, P. (1983): Spinel minerals in transitional and alkali basaltic glasses from Iceland. *Contrib. Mineral. Petrol.* **83**, 141-149.
- TOULMIN, P., III & BARTON, P.B., JR. (1964): A thermodynamic study of pyrite and pyrrhotite. *Geochim. Cosmochim. Acta* **28**, 641-671.
- VON BARGEN, N. & WAFF, H.S. (1986): Permeabilities, interfacial areas and curvatures of partially molten systems. Results of numerical computations of equilibrium microstructures. *J. Geophys. Res.* **91**, 9261-9276.
- WAFF, H.S. & FAUL, U.H. (1992): Effects of crystalline anisotropy on fluid distribution in ultramafic partial melts. *J. Geophys. Res.* **97**, 9003-9014.
- WALLACE, P. & CARMICHAEL, I.S.E. (1992): Sulfur in basaltic magmas. *Geochim. Cosmochim. Acta* **56**, 1863-1874.
- WATSON, E.B. (1982): Melt infiltration and magma evolution. *Geology* **10**, 236-240.
- _____ & BRENNAN, J.M. (1987): Fluids in the lithosphere. 1. Experimentally-determined wetting characteristics of CO₂–H₂O fluids and their implications for fluid transport, host-rock physical properties, and fluid inclusion formation. *Earth Planet. Sci. Lett.* **85**, 497-515.
- _____, _____ & BAKER, D.R. (1990): Distribution of fluids in the continental mantle. In *Continental Mantle* (M.A. Menzies, ed.). Oxford University Press, Oxford, U.K. (111-125).
- _____ & LUPULESCU, A. (1993): Aqueous fluid connectivity and chemical transport in clinopyroxene-rich rocks. *Earth Planet. Sci. Lett.* **117**, 279-294.
- ZHOU, MEI-FU & ROBINSON, P.T. (1997): Origin and tectonic environment of podiform chromite deposits. *Econ. Geol.* **92**, 259-262.
- _____, _____, MALPAS, J. & LI, Z. (1996): Podiform chromitites in the Luobusa ophiolite (southern Tibet): implications for melt–rock interaction and chromite segregation in the upper mantle. *J. Petrol.* **37**, 3-21.

Received January 18, 2002, revised manuscript accepted June 5, 2002.